

DNA-PRIOR: UNSUPERVISED DENOISE ANYTHING VIA DUAL-DOMAIN PRIOR

Yanqi Cheng¹, Chun-Wun Cheng¹, Jim Denholm², Thiago Lima³, Javier A. Montoya-Zegarra^{4,3},
Richard Goodwin², Carola-Bibiane Schönlieb¹, Angelica I Aviles-Rivero^{5*}

¹University of Cambridge, ²Predictive Artificial Intelligence and Data, Clinical Pharmacology and Safety Sciences, AstraZeneca R&D, ³Lucerne University Teaching and Research Hospital, ⁴Zurich University of Applied Sciences, ⁵YMSC, Tsinghua University

ABSTRACT

Medical imaging pipelines critically rely on robust denoising to stabilise downstream tasks such as segmentation and reconstruction. However, many existing denoisers depend on large annotated datasets or supervised learning, which restricts their usability in clinical environments with heterogeneous modalities and limited ground-truth data. To address this limitation, we introduce DNA-Prior, a universal unsupervised denoising framework that reconstructs clean images directly from corrupted observations through a mathematically principled hybrid prior. DNA-Prior integrates (i) an implicit architectural prior, enforced through a deep network parameterisation, with (ii) an explicit spectral-spatial prior composed of a frequency-domain fidelity term and a spatial regularisation functional. This dual-domain formulation yields a well-structured optimisation problem that jointly preserves global frequency characteristics and local anatomical structure, without requiring any external training data or modality-specific tuning. Experiments across multiple modalities show that DNA achieves consistent noise suppression and structural preservation under diverse noise conditions.

Index Terms— Medical Imaging, Inverse Problem, Unsupervised Denoising

1. INTRODUCTION

High-quality medical images are essential for downstream tasks such as segmentation, registration, and reconstruction, yet clinical acquisitions are often insufficiently constrained, due to the complex characteristics of noise and anatomical structures. These degradations can obscure fine anatomical structures and bias quantitative analysis, making effective denoising a critical preprocessing step. Classical methods can suppress noise but often oversmooth important details. Although recent deep learning-based approaches have achieved state-of-the-art performance in CT [1] and MRI [2], denoising across different modalities remains challenging.

Although supervised denoising—particularly deep learning approaches—have produced strong quantitative gains in

CT and MRI, these methods typically depend on large, clean and task-specific training sets whose collection is costly, privacy-constrained, and often impractical. Even when available, models tend to overfit to scanner- or protocol-specific patterns, degrading performance under domain shifts. These issues, combined with heavy computational demands and limited uncertainty estimation, highlight the need for data-efficient denoising approaches that generalise across modalities and noise conditions without requiring paired data [3, 4].

Classical explicit priors such as Total Variation [5], sparsity [6], and smoothness [7] assumptions have long been used to encode well-understood properties of clean medical and natural images. More recently, implicit priors derived from neural networks — most notably Deep Image Prior (DIP) [8] and self-supervised denoising frameworks like Noise2Self [3] — have shown that the architecture of deep models itself can capture powerful structural regularities without paired clean data. Recent studies show that integrating explicit and implicit priors improves denoising robustness and generalisation under real-world noise and distribution shifts by uniting hand-crafted knowledge with data-driven representations [9, 10].

Our contributions are: (1) We formulate a universal unsupervised denoising model in which the reconstruction is constrained to a network-parameterised manifold and estimated solely from the corrupted measurement. (2) We introduce a dual-prior learning framework based on an implicit architectural prior with an explicit spectral-spatial regularisation functional, consisting of a frequency-domain fidelity term and a spatial variation penalty, yielding a well-posed optimisation problem over network parameters. (3) We show that this formulation produces stable, modality-agnostic solutions across heterogeneous noise regimes, demonstrating the effectiveness of the proposed prior structure in medical imaging settings.

2. METHODOLOGY

We propose a **dual-domain denoising framework** that generalises across diverse medical imaging modalities without requiring any annotated data. Unlike supervised approaches, which rely on large paired datasets, our method is entirely unsupervised, exploiting the inherent structure of convo-

*Corresponding Author.

lutional neural networks to capture a substantial portion of image statistics independently of learning. To further enhance reconstruction fidelity, we incorporate complementary regularisation in both the frequency and spatial domains, thereby enforcing spectral consistency and spatial smoothness simultaneously. This hybrid prior formulation provides robust and generalisable denoising performance across varying noise levels and imaging modalities.

Let $\Omega \subset \mathbb{R}^2$ denote the discrete image grid and $x \in \mathbb{R}^{|\Omega|}$ the unknown clean image generating the observation $y = x + \varepsilon, \varepsilon \sim \mathcal{N}(0, \sigma^2 I)$. A standard variational formulation recovers x by solving:

$$\hat{x} = \arg \min_x \{\mathcal{D}(x, y) + \Phi(x)\}, \quad (1)$$

where \mathcal{D} is a fidelity term (e.g., $\|x - y\|_2^2$) and Φ is an explicit regulariser encoding prior knowledge. Classical choices include total variation, sparsity, or wavelet-domain constraints. However, designing Φ suitable for heterogeneous medical modalities is non-trivial.

Recent unsupervised methods replace the explicit prior Φ in (1) with an implicit prior induced by a deep neural network. The underlying assumption is that images lie on a low-dimensional manifold generated by a convolutional architecture. Accordingly, the reconstruction is constrained to the set $\mathcal{M} = \{f_\theta(z) : \theta \in \Theta\}$, where f_θ is a CNN with parameters θ and z is a fixed random input tensor. Thus, instead of optimising over x , the problem becomes

$$\theta^* = \arg \min_\theta \mathcal{D}(f_\theta(z), y), \quad (2)$$

which is the formulation underlying Deep Image Prior [8] (DIP) and Deep Spectral Prior [11] (DSP). In these approaches, the implicit structure of f_θ serves as the sole regularisation mechanism. While effective in certain settings, such fidelity-only implicit priors are insufficient in medical imaging, where noise characteristics and anatomical structures possess modality-dependent spectral and spatial behaviour that is not adequately constrained by (2).

2.1. Denoise Anything via Dual-Domain Objective

In line with implicit priors, we adopt the network parameterisation $\hat{x} = f_\theta(z)$, and view reconstruction as an optimisation over θ . This constrains the solution to the manifold \mathcal{M} defined above. However, instead of relying solely on a fidelity term as in DIP/DSP, we now introduce a dual-domain regularisation strategy that explicitly incorporates both spectral and spatial constraints.

Implicit Prior Domain: Spectral Fidelity Loss. To enforce global spectral consistency between the reconstruction and the measurement, we propose a fidelity term directly in the frequency domain. Let \mathcal{F} denote the discrete Fourier transform and recall that the network-parameterised reconstruction is given by $\hat{x} = f_\theta(z)$. We then introduce the spectral fidelity loss

$$\mathcal{L}_{\text{IS}}(\theta) = \frac{\|\mathcal{F}(f_\theta(z)) - \mathcal{F}(y)\|_2^2}{\|\mathcal{F}(y)\|_2^2 + \gamma}, \quad (3)$$

where $\gamma > 0$ ensures numerical stability.

This loss serves as a domain-consistent alternative to pixel-space fidelity by directly constraining the reconstruction to match the anatomical spectral distribution of the measurement. Importantly, \mathcal{L}_{IS} is fully compatible with the implicit prior induced by the network architecture: while the network enforces structural regularity through its architectural bias, the spectral constraint guides the optimisation toward solutions whose global frequency characteristics remain faithful to the measured data.

Explicit Prior Domain: Spatial Regularisation. To complement the spectral constraint with local spatial structure, we employ an explicit total variation (TV) regulariser. Let D_x and D_y denote discrete finite differences. The γ -smoothed isotropic TV seminorm is defined as

$$\text{TV}(\hat{x}) = \sum_{(i,j) \in \Omega} \sqrt{(D_x \hat{x})_{i,j}^2 + (D_y \hat{x})_{i,j}^2 + \gamma^2}. \quad (4)$$

Following a scale-normalised formulation, we define

$$\mathcal{L}_{\text{TV}} = \frac{\text{TV}(\hat{x})}{\|\hat{x}\|_2^2 + \gamma}. \quad (5)$$

Dual-Domain Optimisation Scheme. Taking the spectral fidelity (3) and spatial regularisation (5), the reconstruction is obtained by solving

$$\mathcal{L}_{\text{total}}(\theta) = \alpha \mathcal{L}_{\text{IS}} + \beta \mathcal{L}_{\text{TV}}, \quad (6)$$

with $\alpha, \beta > 0$ controlling the contributions of the two terms. The optimal parameters are given by

$$\theta^* = \arg \min_\theta \mathcal{L}_{\text{total}}(\theta), \quad (7)$$

and the final reconstruction is $\hat{x} = f_{\theta^*}(z)$.

This formulation integrates implicit architectural priors with explicit spectral and spatial constraints, yielding a mathematically principled dual-domain method that captures the heterogeneous characteristics of medical imaging data.

3. EXPERIMENTAL RESULTS

3.1 Experimental Setup. All experiments were conducted on a workstation equipped with a single NVIDIA RTX 4090 GPU (24 GB VRAM). Each denoising task was performed independently for maximum 3,000 iterations per image without any pretraining or external supervision. Specifically, our DNA-Prior uses parameters $\alpha = 1$ and $\beta = 0.0001$.

Datasets and Noise Settings. To evaluate the generalisation ability of the proposed method, we conducted experiments on seven representative medical imaging modalities: Microscopy [18], MRI [19], PET [20], CT [21], Endoscopy [22], Histopathology (in-house dataset), and Ultrasound [23]. For each modality, synthetic Gaussian noise with

	σ	Wavelet	TV	CBM3D	DIP	DIP-TV	WIRE	DS-N2N	DSP	DNA-Prior
		2000 [12]	2004 [13]	2012[14]	2018 [8]	2019 [15]	2023 [16]	2025 [17]	2025 [11]	2025
Microscopy [18]	15	38.10	40.34	40.75	41.96	41.98	38.33	41.14	41.82	42.11
	25	32.90	32.57	33.09	34.28	34.26	31.59	34.08	34.28	34.32
	50	24.97	24.30	22.54	25.19	25.10	23.03	25.26	25.13	25.31
MRI [19]	15	30.33	31.40	32.80	33.31	33.05	33.55	32.56	33.10	33.69
	25	26.84	27.17	29.29	29.75	29.73	29.67	28.82	29.62	29.76
	50	21.93	20.07	20.85	23.56	23.70	23.99	23.05	23.69	24.02
PET [20]	15	32.28	32.97	32.97	33.11	33.15	32.90	32.61	33.13	33.24
	25	28.48	28.73	28.73	29.12	29.13	28.97	28.97	29.14	29.16
	50	22.83	22.52	21.28	23.20	23.18	23.15	22.81	23.19	23.20
CT [21]	15	28.45	29.66	30.08	30.93	30.95	30.61	31.12	30.92	31.38
	25	25.62	26.64	28.96	29.25	29.18	28.77	28.43	29.21	29.32
	50	21.16	19.89	20.49	23.97	23.84	24.12	23.70	23.96	24.57
Endoscopy [22]	15	32.07	31.24	31.78	32.25	32.42	32.70	32.83	32.42	32.92
	25	29.08	30.41	29.16	26.23	26.97	30.32	30.33	30.48	30.77
	50	24.41	23.85	20.38	23.18	25.49	25.17	24.87	25.43	25.50
Histopathology	15	28.98	28.92	27.28	30.01	29.80	28.77	30.72	30.05	31.22
	25	26.57	28.01	26.61	29.47	29.49	28.10	28.80	29.45	30.11
	50	23.87	23.60	25.11	26.75	26.70	25.64	25.71	26.84	27.13
Ultrasound [23]	15	31.52	33.28	33.42	34.38	34.43	31.89	34.81	34.78	36.54
	25	29.20	30.98	31.55	32.97	34.05	31.33	32.45	33.29	34.40
	50	26.33	24.47	27.75	30.17	30.02	28.44	28.85	30.07	30.27

Table 1. Comparison of our method on PSNR (dB) with classical and unsupervised baselines, including Wavelet [12], TV [13], CBM3D [14], DIP [8], DIP-TV [15], WIRE [16], DS-N2N [17], and DSP [11], all tested under identical noise settings.

standard deviations $\sigma = 15, 25, 50$ was added to simulate different degradation levels. Only noisy images were used during optimisation, while clean images were reserved for quantitative evaluation.

Evaluation Metric. The denoising performance was assessed using the Peak Signal-to-Noise Ratio (PSNR), which is the mean squared error between the denoised output and the clean ground truth. Higher PSNR values indicate better denoising quality and higher fidelity to the original image.

3.2 Results and Discussion Quantitative and qualitative results across all modalities and noise levels are reported in Table 1, and Fig. 1 respectively. Methods relying purely on explicit priors, such as Wavelet [12], TV [13] and CBM3D[14], achieve reasonable noise suppression but tend to oversmooth fine anatomical structures due to their limited modeling capacity. Implicit-prior methods, including DIP [8], DSP [11] and WIRE [16], better preserve high-frequency textures by exploiting image-specific structural regularisation, yet introduce residual artifacts or inconsistent contrast in complex regions. Hybrid techniques, such as DIP+TV [15], and DS-N2N [17], leading to more balanced reconstructions under complex imaging scenario across all 7 modalities. Our proposed method, which further integrates an adaptive explicit regulariser with a spectral implicit prior, consistently achieves the highest PSNR across all datasets. Notably, substantial improvements are observed for CT and Ultrasound modalities, where balancing smoothness and detail preservation is particularly challenging. As shown in Fig. 1, our hybrid prior

framework effectively suppresses noise while maintaining structural fidelity and contrast, outperforming both traditional and purely data-driven zero-shot denoising approaches.

Quantitative Results. A closer examination of Table 1 reveals several consistent trends across modalities and noise levels. As the noise level σ increases from 15 to 50, the PSNR of all methods naturally declines, reflecting the greater denoising difficulty. Among the baselines, explicit-prior methods (Wavelet, TV and CBM3D) exhibit significant performance drops at high σ , demonstrating their limited capacity to model complex noise distributions. Implicit-prior approaches (DIP, WIRE) perform competitively at lower noise levels but tend to overfit to noise patterns with low PSNR. Hybrid methods, such as DIP-TV, show improved consistency, validating the advantage of combining structural smoothness with learned priors. Notably, our approach achieves the highest PSNR on all modalities, with particularly strong gains in CT and Ultrasound images—modalities known for high-frequency texture and speckle noise. These results highlight that the proposed hybrid prior not only enhances denoising fidelity but also generalises effectively across diverse imaging domains without external training data.

Qualitative Results. In addition to the quantitative analysis, Fig. 1 presents qualitative comparisons across multiple modalities for the challenging case of $\sigma = 50$. At this high noise level, all methods exhibit some loss of fine structural details. Explicit-prior approaches fail to adequately suppress noise, resulting in residual artifacts that obscure subtle tex-

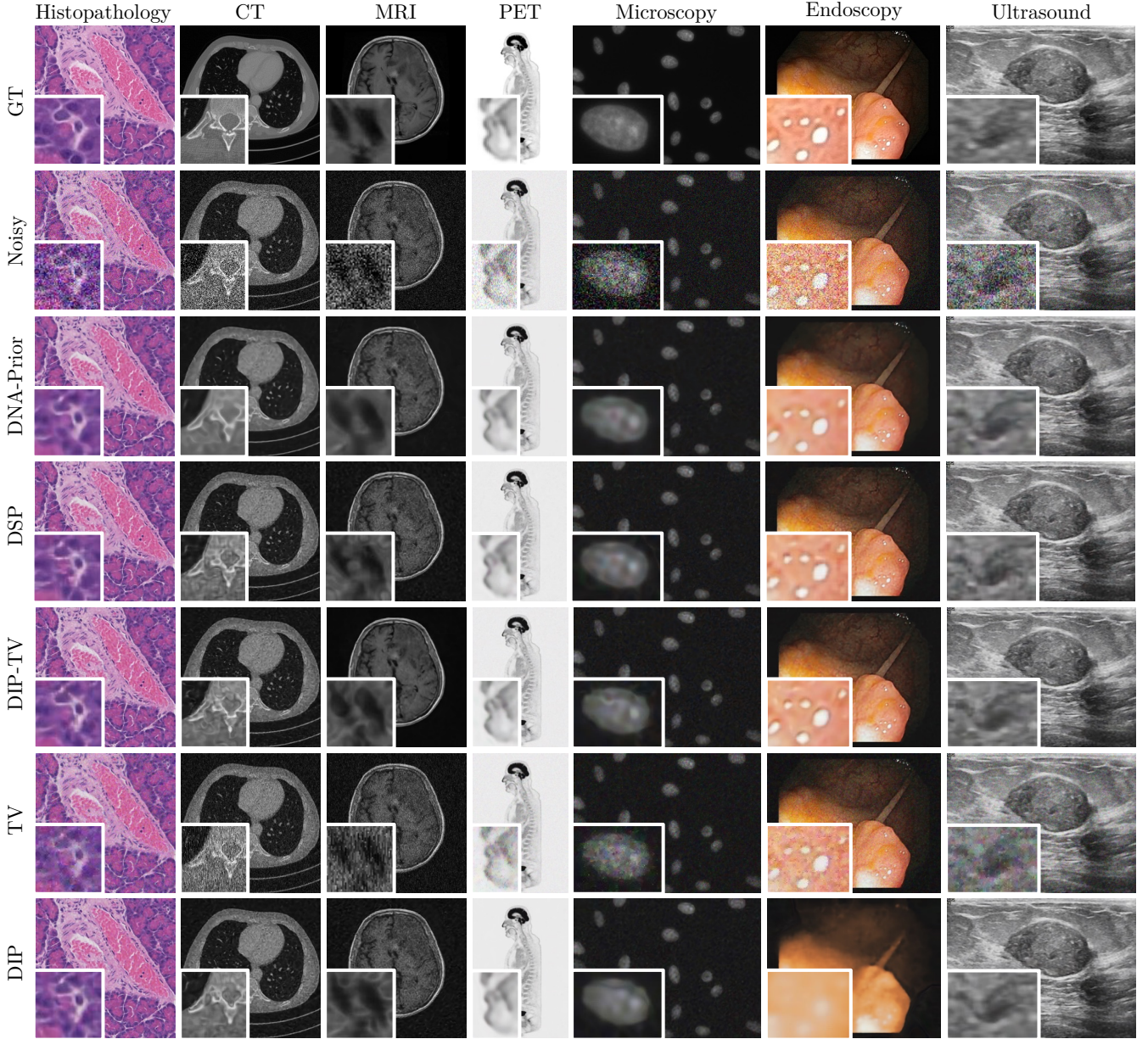


Fig. 1. Visual comparison of denoising results for $\sigma = 50$, showing DNA-Prior versus existing state-of-the-art methods.

tures. In the histopathology modality, while most methods reconstruct the overall tissue structures, fine cellular boundaries and morphological details are either over-smoothed or distorted. Purely implicit-prior methods (DIP, DSP) recover finer textures but occasionally introduce twisted patterns, a phenomenon also observed in the Ultrasound modality. Other hybrid or learning-based baselines sometimes generate additional spurious patterns that deviate from the true anatomical structures. In contrast, our proposed method effectively removes noise while faithfully preserving realistic structural and textural information across all modalities, demonstrating superior generalisation under severe degradation.

4. CONCLUSION

We introduced DNA-Prior, a universal unsupervised denoising framework combining an implicit architectural prior with explicit spectral–spatial regularisation. The resulting learning formulation reconstructs clean images directly from corrupted measurements while preserving frequency structure and anatomical detail. Experiments across multiple modalities demonstrate stable and generalisable performance, supporting its utility in medical imaging workflows. Future work includes investigating the performance of the method under different types of clinically relevant, modality-specific noise.

5. COMPLIANCE WITH ETHICAL STANDARDS

This research study was conducted retrospectively using human subject data made available in open access. Ethical approval was not required as confirmed by the license attached with the open access data.

6. ACKNOWLEDGMENT

YC is funded by an AstraZeneca studentship and a Google studentship. CWC, JAMZ and AIAR acknowledge support from the Swiss National Science Foundation (SNSF) under grant number 20HW-1 220785. CBS acknowledges support from the Philip Leverhulme Prize, the Royal Society Wolfson Fellowship, the EPSRC advanced career fellowship EP/V029428/1, EPSRC grants EP/S026045/1 and EP/T003553/1, EP/N014588/1, EP/T017961/1, the Wellcome Innovator Awards 215733/Z/19/Z and 221633/Z/20/Z, the European Union Horizon 2020 research and innovation programme under the Marie Skłodowska-Curie grant agreement No. 777826 NoMADS, the Cantab Capital Institute for the Mathematics of Information and the Alan Turing Institute. AIAR gratefully acknowledges the support from Yau Mathematical Sciences Center, Tsinghua University. This work is also supported by the Tsinghua-PolyU Joint Research Initiative Fund and the Tsinghua University Dushi Program.

7. REFERENCES

- [1] Elias Eulig, Björn Ommer, and Marc Kachelrieß, “Benchmarking deep learning-based low-dose ct image denoising algorithms,” *Medical physics*, vol. 51, no. 12, pp. 8776–8788, 2024.
- [2] Shutian Zhao, Fan Xiao, James F Griffith, Ruokun Li, and Weitian Chen, “Denoising of volumetric magnetic resonance imaging using multi-channel three-dimensional convolutional neural network with applications on fast spin echo acquisitions,” *Quantitative Imaging in Medicine and Surgery*, vol. 14, no. 9, pp. 6517, 2024.
- [3] Joshua Batson and Loic Royer, “Noise2self: Blind denoising by self-supervision,” *ICML*, 2019.
- [4] Zejin Wang, Jiazheng Liu, Guoqing Li, and Hua Han, “Blind2unblind: Self-supervised image denoising with visible blind spots,” in *Proceedings of the IEEE/CVF conference on computer vision and pattern recognition*, 2022, pp. 2027–2036.
- [5] Leonid I Rudin, Stanley Osher, and Emad Fatemi, “Nonlinear total variation based noise removal algorithms,” *Physica D*, 1992.
- [6] David L Donoho, “De-noising by soft-thresholding,” *IEEE Trans. Information Theory*, 1995.
- [7] Andrey N Tikhonov and Vasiliy Y Arsenin, *Solutions of Ill-posed Problems*, 1977.
- [8] Dmitry Ulyanov, Andrea Vedaldi, and Victor Lempitsky, “Deep image prior,” in *Proceedings of the IEEE conference on computer vision and pattern recognition*, 2018, pp. 9446–9454.
- [9] Kai Zhang, Wangmeng Zuo, et al., “Plug-and-play methods for image restoration: A survey,” *IEEE Signal Processing Magazine*, 2021.
- [10] Singanallur V. Venkatakrishnan, Charles A. Bouman, and Brendt Wohlberg, “Plug-and-play priors for model based reconstruction,” in *IEEE GlobalSIP*, 2013.
- [11] Yanqi Cheng, Xuxiang Zhao, Tieyong Zeng, Pietro Lio, Carola-Bibiane Schönlieb, and Angelica I Aviles-Rivero, “Deep spectral prior,” *arXiv preprint arXiv:2505.19873*, 2025.
- [12] S Grace Chang, Bin Yu, and Martin Vetterli, “Adaptive wavelet thresholding for image denoising and compression,” *IEEE transactions on image processing*, vol. 9, no. 9, pp. 1532–1546, 2000.
- [13] Antonin Chambolle, “An algorithm for total variation minimization and applications,” *Journal of Mathematical imaging and vision*, vol. 20, pp. 89–97, 2004.
- [14] Marc Lebrun, “An analysis and implementation of the bm3d image denoising method,” *Image Processing On Line*, vol. 2, pp. 175–213, 2012.
- [15] Jiaming Liu, Yu Sun, Xiaojian Xu, and Ulugbek S Kamilov, “Image restoration using total variation regularized deep image prior,” in *ICASSP 2019-2019 IEEE International Conference on Acoustics, Speech and Signal Processing (ICASSP)*. Ieee, 2019, pp. 7715–7719.
- [16] Vishwanath Saragadam, Daniel LeJeune, Jasper Tan, Guha Balakrishnan, Ashok Veeraraghavan, and Richard G Baraniuk, “Wire: Wavelet implicit neural representations,” in *Proceedings of the IEEE/CVF Conference on Computer Vision and Pattern Recognition*, 2023, pp. 18507–18516.
- [17] Jibo Bai, Daqi Zhu, and Mingzhi Chen, “Dual-sampling noise2noise: Efficient single image denoising,” *IEEE Transactions on Instrumentation and Measurement*, 2025.
- [18] Juan C Caicedo, Allen Goodman, Kyle W Karhohs, Beth A Cimini, Jeanelle Ackerman, Marzieh Haghghi, CherKeng Heng, Tim Becker, Minh Doan, Claire McQuin, et al., “Nucleus segmentation across imaging experiments: the 2018 data science bowl,” *Nature methods*, vol. 16, no. 12, pp. 1247–1253, 2019.
- [19] Msoud Nickparvar, “Brain tumor mri dataset,” 2021.
- [20] Kuangyu Shi, Rui Guo, Song Xue, Axel Rominger, and Biao Li, “Ultra-low dose pet imaging challenge 2022,” Mar. 2022.
- [21] Brad Albertina, Mark Watson, Chandra Holback, Rose Jarosz, Shanah Kirk, Yueh Lee, Kimberly Rieger-Christ, and John Lemmerman, “The cancer genome atlas lung adenocarcinoma collection (tcga-luad),” 2016.
- [22] Debesh Jha, Pia H Smedsrød, Michael A Riegler, Pål Halvorsen, Thomas De Lange, Dag Johansen, and Håvard D Johansen, “Kvasir-seg: A segmented polyp dataset,” in *International conference on multimedia modeling*. Springer, 2019, pp. 451–462.
- [23] Walid Al-Dhabayani, Mohammed Gomaa, Hussien Khaled, and Aly Fahmy, “Dataset of breast ultrasound images,” *Data in brief*, vol. 28, pp. 104863, 2020.